Urban Zero-Emission Aerial Transportation: Design and Analysis of a Short-Takeoff-and-Landing UAV Based on Tilted Boundary Layer Ingestion Engines

Authors: Hanyue Shen, Ningzi Chen

Shanghai Pinghe School, Chongqing Yucai Middle School

People's Republic of China

Urban Zero-Emission Aerial Transportation: Design and Analysis of a Short-Takeoff-and-Landing UAV Based on Tilted Boundary Layer Ingestion Engines

1st Hanyue Shen

Shanghai Pinghe School

People's Republic of China

2nd Ningzi Chen

Chongqing Yucai Middle School

People's Republic of China

Abstract—The growing express delivery industry is a reflection of the blooming economy, yet it also comes with a significant cost: carbon emission. This research explores a method to mitigate this pollution – using unmanned eSTOL freights to carry out branch line transportation, replacing trucks. By innovatively developing a tilted electric boundary layer ingestion propulsion system using VLM, CFD, and experimental methods, a UAV capable of operating under urban scenarios is designed, achieving a remarkable 16.09% increment in lift, 13.90% conservation in energy compared to conventional solutions, while conserving 9.40% energy in climb, shedding a new light to the application of low-altitude aerial industry in reducing carbon emissions and improving transportation efficiency.

Keywords—Boundary Layer Ingestion, Distributed Propulsion System, eSTOL, Computational Fluid Dynamics, System Engineering, Low Altitude Airspace Economy.

Table of Abbreviations	
aoa	Angle of Attack
BLI	Boundary Layer Ingestion
EDF	Electric Ducted Fan
STOL	Short Takeoff/Landing
UAV	Unmanned Aerial Vehicle

I. Introduction

A. Initiative

Express delivery has grown to become a major part of urban lives nowadays. However, its convenience is at a significant environmental cost. In 2022 alone, China has reported an emission of 55.65 million tons of carbon dioxide emission by express industry, making a 3.4% growth compared to the previous year. Almost 63% of this emission was contributed by transportation sequences [1].

Road transportation contributed 85% precent of the transportation-related emissions (18.74 million tons in

2022) [1]. According to CEIC, the average road transportation distance is 185.774km in 2022 [2]. This distance is classified under short range by definition.

If a zero-emission solution can mitigate the carbon dioxide resulted by road transportation while maintaining the transportation efficiency and capability, the emission levels of the express industry can be significantly reduced by adopting the replacement. This project is hence dedicated to developing such a solution with unmanned aerial vehicles (UAVs).

B. Background Information and Previous Research

The blooming of low-altitude airspace industry global wide has resulted in numerous advancements in propulsion layouts – one of which is the boundary layer ingestion (BLI) engines.

BLI engines are typically placed on trailing sections of the airfoil. Aside from providing thrust, these engines create artificial low-pressure zones near their intake areas to accelerate the airflow on the upper airfoil [3][4]. It is believed to be a promising method that decreases aircraft thrust power consumption and thus reducing fuel consumption [5]. NASA has publicized its research on large-scale BLI systems in 2019, indicating a possible 3-5% decrease in fuel usage with its D8 series design [6]. The German startup company Lilium Jet had also successfully tested their electric vertical-takeoff-and-landing (eVTOL) solution based on BLI technology in 2023.

Existing studies on BLI engines provide solutions with horizontally aligned engine layouts. However, the team believes that tilted installation – along approximate tangential orientations relative to the airfoil – can potentially take the efficiency BLI technology to a higher level. Meanwhile, tilted propulsion is also a suitable candidate for urban flights, being a mix between multirotor and fix-winged layouts in terms of both force layout and performance.

With this background, this research is dedicated to the development of a novel tilted electric BLI propulsion system and demonstrating its implementation in the given scenario of branch line logistics.

C. Hypothesis and Goal

The research evolves around the hypothesis that tilted BLI layout is more efficient than existing UAV solutions including other BLI systems and conventional layouts, and that it is suitable for urban branch line transportation missions.

The purpose of the design is to provide a more efficient zero-emission airspace system solution that replaces current branch line transportation methods in order to mitigate carbon emissions caused by the process.

D. Design Requirements

To devise a design solution fitting the requirements of the given scenario, several numerical constraints (minimal requirements) are set, as explained below with their respective justifications.

Payload Capacity: MTOW is 40kg, with an effective payload of 16kg based on humans' carrying weight limit [7]. The payload ratio is 40%, exceeding market competitors such as FlyCart (32% [8]).

Cruise Specifications: the UAV is designed to carry out branch line flights. Take Shanghai as reference, the distance between Jinshan District and Baoshan District is over 80km. Set the minimal cruise distance with payload be *95km* (85% rule). With a standard cruising speed of *20m/s*, the minimal acceptable endurance is estimated to be *1.32hrs*.

Takeoff and Landing: The UAV is designed to take off at areas analogous to a middle school soccer yard approximately 65 meters in length [9]. Taking the height distribution of Shanghai's buildings, the UAV must be able to climb up to *80 meters* in altitude shortly after takeoff [10]. According to local 1:1.2 rule [11], this gives a minimal *climb rate requirement of 1:1.5* or climbing at *33.7 degrees*.

Wingspan: due to the restriction of landing and takeoff area, with reference to the six lanes on 200m courts that are 1.22 meters wide each [12] for standard fields, the (maximum) wingspan is placed at at *4880mm* – 2/3 of the runway width.

Noise Levels: noise levels heard by observers at ground level (at least 80m away) must be under the disturbance limit – less than 50dBA to 55dBA [13]. Comparatively, general consumer model UAVs produce noise levels at 70 to 81dBA [13], while the level for larger UAVs can reach up to 96dBA [14].

II. METHODOLOGY

A. Assumptions and Simplifications

During the design and calculation processes, the following pre-requisites are set in order for calculation purposes.

- Assume the EDF engine to be an *airflow accelerator* (in simulation processes) with given wind speed increment at designated input voltage.
- Assume the use of *straight, rectangular wings* as main lifting surfaces during the design with no tip twisting.
- Assume linear energy-thrust relation in rotors.

B. Theoretical Basis

During the design process, aside from analytic calculations, the main tools used include Vortex-Lattice Method with Ring Vortex, Finite Element Analysis, and wind tunnel experiment.

Two important formulae used in the calculations are the modern lift and drag formula, given by:

$$F_{lift} = \frac{1}{2}\rho S C_l V^2, (1\text{A})$$

$$F_{drag} = \frac{1}{2}\rho S C_d V^2. (1\text{B})$$

Define the EDF orientation angle θ to be the angle between the horizontal orientation and the axis of the EDF, and hence the nominal installation angle of the EDFs is given by $\theta - \alpha$. Using equilibrium of the forces, the following relations can be established.

$$F_{thrust} = \frac{1}{2} C_d \rho S V^2 \sec\theta\,, (2\text{A})$$

$$F_{lift} = \frac{1}{2}\rho S V^2 (C_d \tan\theta + C_l) = W. (2\text{B})$$

W is the weight of the aircraft in Newtons. Given the takeoff weight of the UAV, the thrust can be represented in terms of the orientation angle. In the distributed thrust case, the force is consisted of output forces in multiple smaller units. Hence, a related equation can be derived.

Assuming that there are n EDFs and it is desired that they operate at a certain throttle level T (between 0 to 1), the maximum thrust force required of the EDFs can be found using the relation:

$$F_{unit} = \frac{\mathrm{WC_d}}{nT\sqrt{C_l^2 + C_d^2}} \csc(\theta + \tan^{-1}\frac{C_l}{C_d}). (3)$$

This formula is instructive when selecting the type of EDFs to be used for the design. Introduce the lift-drag ratio R, the above relation can be rewritten.

$$F_{unit} = \frac{\mathrm{W}}{nT\sqrt{R^2 + 1}} \csc(\theta + \tan^{-1} R). (4)$$

This relation will eventually give an instructive function for finding the optimal orientation angle.

The lift and drag equations also help derive the takeoff taxi distance, as the end state of this process can approximated with an equilibrium.

$$d_{taxi} = \frac{V_f^2}{2\left(F_{thrust} - F_{drag} - f\right)}. (5)$$

f is the kinetic friction force given by $f = \mu F_N$. The final velocity F_f must generate enough lift so that the lift force can exactly cancel out with the weight of the aircraft.

These are the equations utilized in the analytic discussions. The equations related to the CFD calculations will be briefly explained below.

The Vortex-Lattice Method (VLM) is a developed calculation method for aerodynamic estimations, mainly accurate for lift calculations and widely applied. The core of the VLM method is the equation of surface boundary condition for inviscid flow:

$$\boldsymbol{V} \cdot \nabla F(x, y, z) = 0, (6)$$

F describes the three-dimensional surface of the wing, whereas the velocity vector $\boldsymbol{V}$ is calculated from

the addition of the incoming velocity, V_∞, and the induced velocity – the derivation of which dependent on the choice of vortex type. The classical VLM method uses the horseshoe vortex, while this research uses a more contemporary ring vortex method.

The FEA simulation uses the Navier-Stokes equation. Assuming constant viscosity flow, the equation is expressed as:

$$\frac{\rho d\boldsymbol{V}}{dt} = \rho F_{ext} - \nabla p + \mu\nabla^2\boldsymbol{V} + \frac{1}{3}\mu\nabla(\nabla\cdot\boldsymbol{V}). (7)$$

p(x,y,z,t) is the position vector in space and F_{ext} is the net external force on fluid – in this case the gravitation ρg and the force provided by the EDFs. For incompressible fluids, the equation can be reduced to:

$$\frac{\rho d\boldsymbol{V}}{dt} = \rho F_{ext} - \nabla p + \mu\nabla^2\boldsymbol{V}. (8)$$

And finally, the set of theoretical equations for calculating noise levels derives the overall noise estimation for the UAV based on empirical data on unit propulsion noise measured at an initial distance d_0.

$$I_0 = I_{unit} + 10\log n,$$

Hence using the six-dB law [15], the noise perceived by observers on the ground at any given cruising height can be derived:

$$I_g = I_0 - 6\cdot\log_2\frac{h_{cruise}}{d_0}.$$

This allows a determination of whether the noise level of the UAV is acceptable.

All related foundational equations have been given and explained above.

C. *Airframe Design*

The lift calculation from XFLR5 yields the following wing initial design (without winglets).

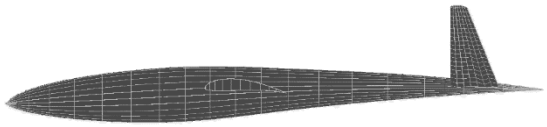

Figure 1. Airframe portside view.

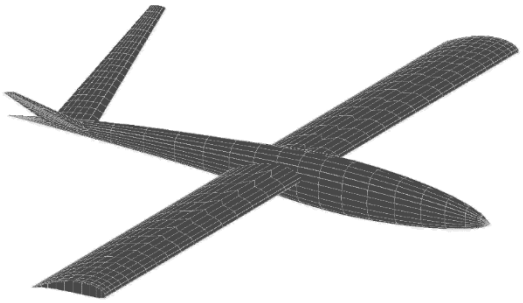

Figure 2. Airframe slanted view.

The wingspan is *4880mm* and the aspect ratio is 9.76, with a tail volume of 0.357. The optimal lift-drag ratio is 18.0, which will be further augmented with BLI engines.

Recall that the required maximum climbing angle is 33.7 degrees. Plotting the lift-drag ratio against lift force will derive the calculation points.

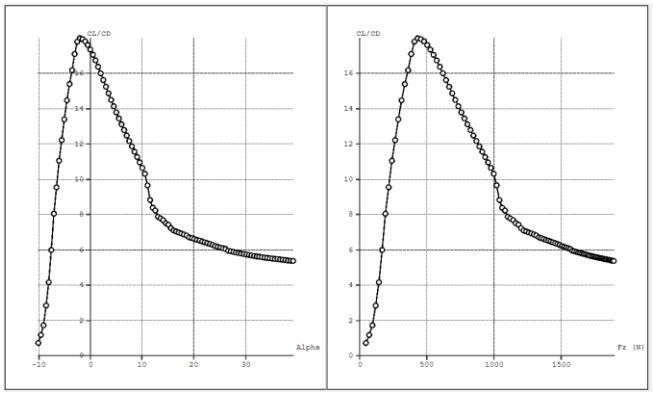

Figure 3. Relations between aoa and lift with the lift-drag ratio.

At 33 degrees, the lift-drag ratio is approximately 5.7. However, empirically, it is known that VLM tends to

underestimate the drag. Hence, the real *R* is likely to be between 2 and 3.

D. Simulation Processes

FEA simulations were carried out in order to optimize the BLI parameters.

The boundary layer ingestion engine creates a negative pressure zone at the opening of the ducted fan, hence accelerating the airflow along the upper surface of the airfoil in front of the EDF. Therefore, the negative pressure zone on the upper surface of the airfoil is enlarged, creating more lift while also generating more downward pitching moment. BLI will also delay the airflow separation on airfoil due to its ingestion, hence it will improve stall properties of the wing and delay the stalling angle, which is certainly required since a large climbing angle is expected at takeoff.

However, the BLI engine also denies certain areas of the wing to create lift. While the EDF will cover up certain sections of the wing, the turbulent wind it outputs will cause a sharp increase in shear pressure on the wing if applied to the upper surface and will cause a loss in lift.

Hence, the BLI must neither be too far to the front nor too far to the back.

Dividing positions as percentage of the Mean Aerodynamic Chord, the researchers ran three simulations to compare different positions at which the BLI engines are placed. Positions -2.5%, 5%, and 12.5% relative to the trailing edge are studied with two sample points taken for the local flow velocity and dynamic pressure values. The eventual solution is also simulated more precisely to gain pressure difference data to evaluate lift increment as a result of the BLI technology.

The simulations are carried out under the conditions of a 20 m/s flow field and 35 m/s EDF exhaust speed. The important data from the figures taken at two points (above 80% M.A.C. and maximum camber position) as the sample locations is collected.

E. Experiment Design

The purpose of wind tunnel experiment is to *validate* simulated data and ensure that the results are accurate rather than to generate new results.

The wind field is generated by the researchers' ϕ0.48 desktop wind tunnel. A brief engineering plot of the device is shown below.

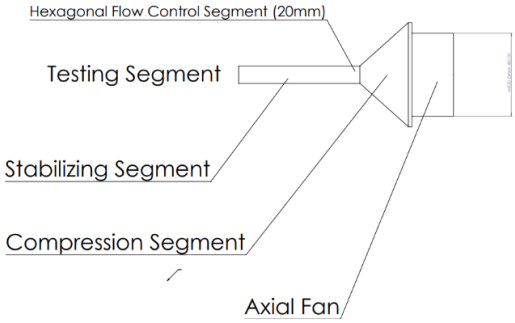

Figure 4. Desktop Wind Tunnel engineering specifications.

The installation consists of a contraction segment, a rectifying segment (hexagonal aluminum grids), and a stabilizing segment, giving a 100mm to 200mm flow outlet as the open testing segment. The axial fan is able to produce a relatively stable flow of up to 4.2 m/s.

A model of the wing with 5% BLI installation position and 100mm M.A.C. was manufactured by 3D printing technology with PLA Silk material. A 35mm diameter EDF is installed and controlled with a 20A ESC connected to an Arduino UNO board, receiving serial port commands from the computer with a mini USB cable. The power supply of the rotor comes from a 4S 4500mAh Li-Po battery.

The combination is fixed into position with an effective *aoa* of 9 degrees by a German equatorial telescope mount in order to provide accurate fixation of the tested model in the flow field.

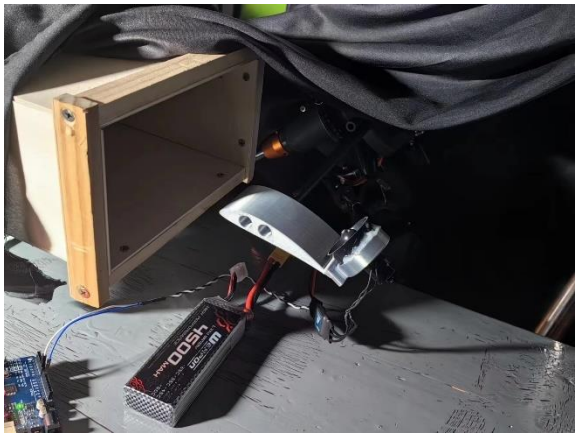

Figure 5. Close-up view of the testing segment.

A smoke cake is used to visualize the flow. When utilizes, it is ignited and led into the testing segment all the way from the inhaling position of the axial fan.

Figure 6. Demonstration of entire experimental equipment.

The model is tested under five different BLI rotation speeds (with serial port signals 1000 to 1400 with 100 interval) and five separate trials are carried out to take the average of the measurements. Data was collected by a hand-held high-accuracy anemometer when experiment starts.

Due to the lack of direct measurement measures, four separate points are selected as sample values for wind speed measurement and validation. One of the points is the measurement of the actual flow field velocity, and the other three are distributed as shown below.

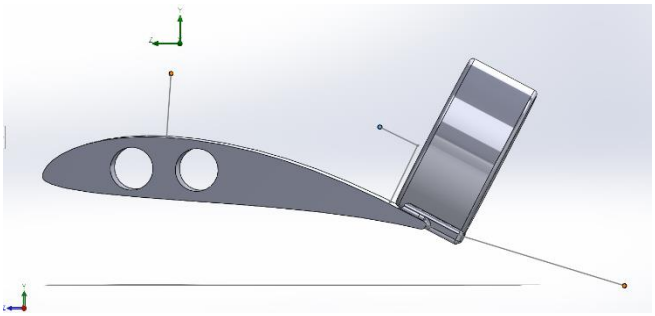

Figure 7. Sample points demonstration.

These three points allow a study of both the boundary layer change, the inhale position conditions, and the trailing flow conditions, thus gaining a relatively thorough view of the case with minimal numbers of samples.

F. Workflow

The entire process of design is summarized by the following plot.

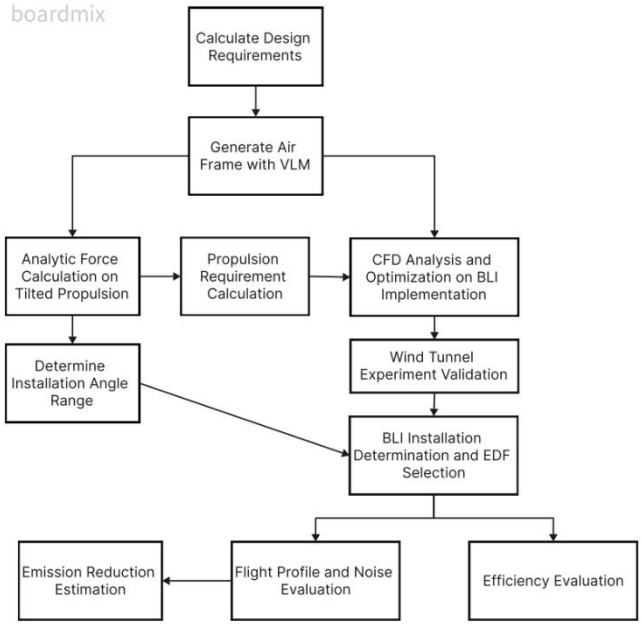

Figure 8. Flow Chart of Design Workflow.

III. RESULTS

A. Force Analysis Insights

We estimate the lift force provided if all of the propulsion vector is along the horizontal direction – that is, a conventional fix-winged layout.

$$F_{unit} = \frac{F_{drag}}{nT} = F_{lift} \cdot \frac{C_d}{nTC_l} = \frac{W}{nTR}.$$

In terms of propulsion power, the relation can be established that:

$$\frac{F_{unit-horz}}{F_{unit-tilt}} = \frac{\sqrt{R^2+1}}{R}\sin(\theta + \tan^{-1} R).$$

It has been calculated that the MH-113 has a maximum R value of over 115 under considered cruising velocity range. In such cases:

$$\frac{\sqrt{R^2+1}}{R} \approx 1,$$

$$\tan^{-1} R \approx \frac{\pi}{2},$$

$$\frac{F_{unit-horz}}{F_{unit-tilt}} \approx \cos(\theta)$$

In this case, the ratio shall be maximized in order for best propulsion efficiency, and hence with this approximation yields a best ratio of 1. Therefore, under high-efficiency cruising, in terms of energy, tilted propulsion is not advantageous.

However, under lower-efficiency cases (either undesired *aoa* or undesired speed), $\boldsymbol{R}$ takes a relatively small value, and hence the factor before sine will be apparently larger than 1. To maximize the ratio for best energy efficiency hence, the optimization strategy is:

$$\sin(\theta + \tan^{-1} R) \to 1,$$

And since the tilting angle is limited between 0 to 90 degrees, and when $\boldsymbol{R}$ is small, the arctangent value is also close to 0, then

$$\theta = \frac{\pi}{2} - \tan^{-1} R.$$

Hence we limit that

$$0 \leq \tan^{-1} R \leq \frac{\pi}{2}.$$

Knowing that the arctangent function can never reach the upper bound, we can make the following assertion in terms of power concerning tilted propulsion layout: the tilted propulsion layout is always less energy consuming than horizontal propulsion as long as the lift-drag ratio of the wing is positive; the advantage of the tilted propulsion reduces as the lift-drag ratio of the wing increases.

The relation between the installation angle and the lift-drag ratio of the entire wing can be plotted.

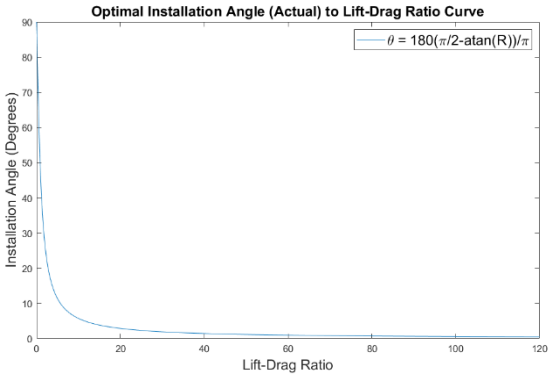

Figure 9. The optimal tilting angle with lift-drag ratio plot.

This provides guidance to the placement of the EDF propeller combined with given data concerning the airframe. While the climb angle required under common situations is slightly over 30 degrees, design safety margins will require a maximum climbing angle at over 40 degrees. Hence the optimal $\boldsymbol{\theta}$ value shall be placed around 40 to 50 degrees, which places the desired nominal installation angle between 10 to 20 degrees (recall that aoa must also be taken into calculation here). An installation angle of *17.64 degrees* is eventually chosen combining BLI flow field concerns.

With previously given force calculations, this conserves 1.11% of climbing energy while maintaining the same efficiency.

In terms of speed, a case study with 600mm*1600mm wing with 64mm EDFs is ran and lift generated at different velocities are shown.

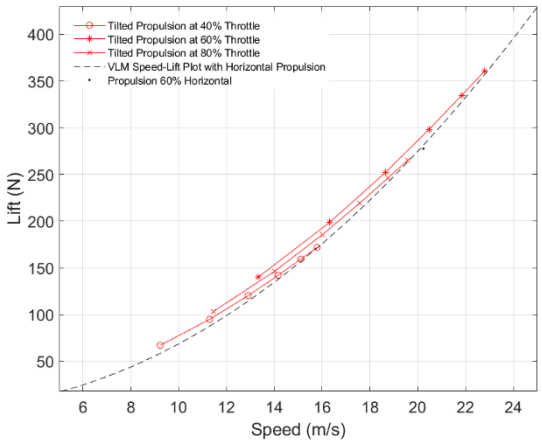

Figure 10. Speed-Lift plot comparing tilted propulsion and fix-winged solution.

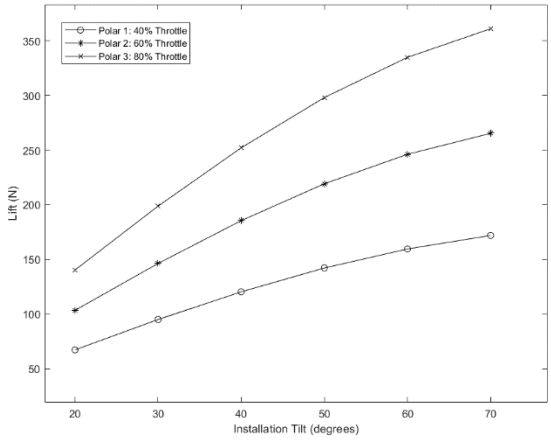

Figure 11. Tilted installation angle (complementary to nominal installation angle) to lift force plot.

Under this context, the tilting angle in the plots refer to the angle between the normal direction and the axis of the EDF, which is the complementary angle of the installation tilt angle mentioned previously in this research. It can be shown that with respect to speed, payload, and lift, the tilted propulsion solution is a compromise between multirotor and fix-winged solutions. Under the same velocities, the tilted propulsion can gain up to *20% more lift* than fix-winged solutions.

According to this methodology, the eventual solution chosen reduces the required climbing airspeed by *3.055%*. That is, the energy efficiency is increased by *9.40%*, as less energy will be required to generate the same amount of lift.

While fix-winged solutions are more aerodynamically efficient and faster, multirotor solutions are slow but heavy, the tilted propulsion solution offers a relatively slow but heavy system design, which complies with the necessities of freight drones used for branch line missions.

B. Propulsion Selection

Using the formula derived, and given the weight of the UAV being 392.4N, taking an installation angle of 15 degrees will help approximate the forces required.

$$F_{unit} = \frac{392.4}{n \cdot 60\% \sqrt{18^2 + 1}} \cdot \csc(0.262 + \tan^{-1} 18)$$

Simplifying the equation:

$$n \cdot F_{unit} = 37.067 \approx 37.1N.$$

Considering the choice of EDF solutions, a set of data of usable EDFs with related data are given. Note that a 5mm gap is assumed between each ducted fan.

Table 1. Types of EDFs with important data.

Aperture	Radius	Force	No.	Thrust
40 mm	50.5 mm	0.264 kg	88	23 kg
50 mm	65 mm	0.480 kg	74	35 kg
55 mm	58.3 mm	0.522 kg	76	40 kg
64 mm	78.2 mm	0.720 kg	66	47 kg
70 mm	84 mm	0.566 kg	54	31 kg
120 mm	136 mm	10.3 kg	34	350 kg
120 mm	136 mm	10.3 kg	16	165 kg

The data are taken from official source at *DWHobby* [16] – one of the major manufacturers of EDF engines, and an additional source [17].

The current used can be calculated by:

$$I_{total} = \frac{37.1N}{F_{max}} \cdot I_{max}$$

Hence to compare energy, the ratio of the maximum current and maximum force must be minimized. Under 3S battery, the ratios of the viable solutions (marked in red) are listed below.

Aperture	Ratio (A/N)
55 mm	53.07

64 mm	58.06
120 mm	5.9

To conserve energy, the 120 mm solution shall be used with 16 units (which provides already ample thrust for the aircraft). High-voltage-low-current strategy is used in order to maximize the use of payload capacity for fuel. A large number of propellers are used while each are engaged with low operational levels. With 24S batteries, the current required for cruise would be:

$$37.1N \cdot \frac{5.9}{4} \cdot 16 = 23.6A.$$

To satisfy the 1.32 hours cruise requirement, the total battery capacity should be 12S 28000+10000mAh [18], summing to a total weight of 6283g for the power batteries.

Each propeller weighs 290g and the corresponding 160A ESC 232.8g (one ESC for three propellers, one group of two on each side), giving a total of 7433.6g for the propulsion avionics, and summing to a total of *13716.6g* dedicated to propulsion.

C. Simulation Results

The dynamic pressure and velocity plots of the discussed cases are shown below.

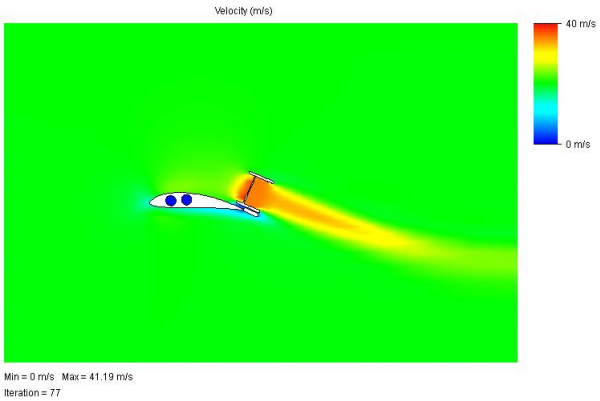

Figure 12. Velocity cut plot of BLI at -2.5% position.

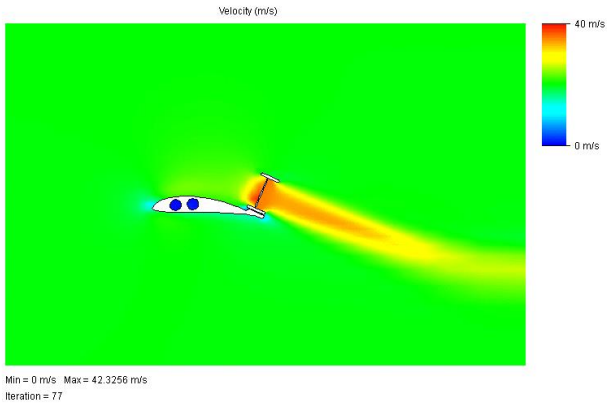

Figure 13. Velocity cut plot of BLI at 5% position.

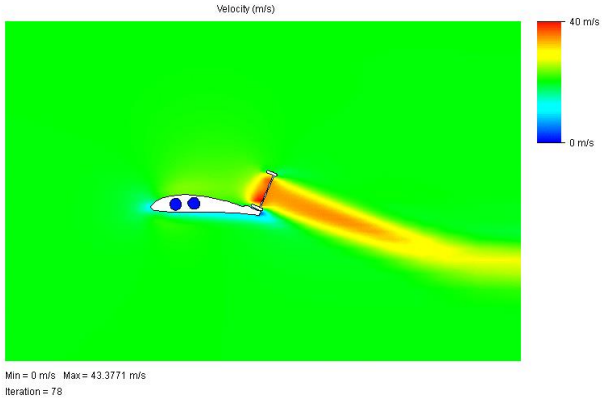

Figure 14. Velocity cut plot of BLI at 12.5% position.

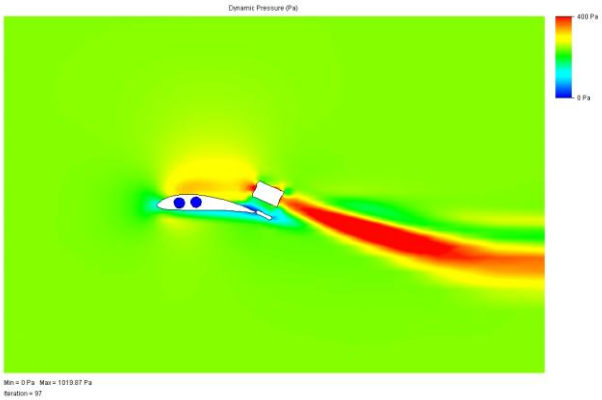

Figure 15. Dynamic pressure cut plot of BLI at -2.5% position.

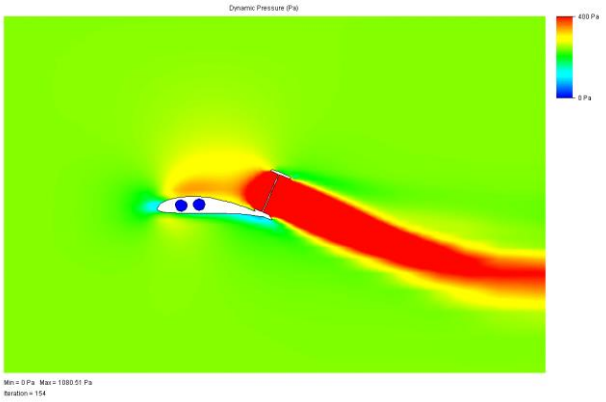

Figure 16. Dynamic pressure cut plot of BLI at 5% position.

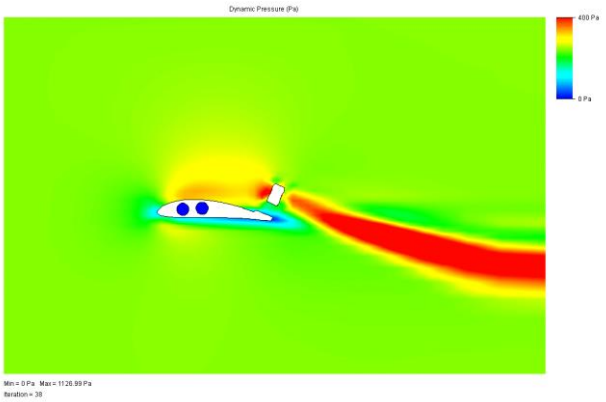

Figure 17. Dynamic pressure cut plot of BLI at -2.5% position.

Important data from sample points are given below.

BLI Pos	V1 (m/s)	V2 (m/s)	DP1 (Pa)	DP2 (Pa)
-2.5%	22.8130	26.0701	313.203	416.110
5%	22.8218	26.2881	313.388	416.961
12.5%	22.8046	26.2857	312.908	416.380
No BLI	22.6594	21.4224	308.990	276.192

The first sample point studies a section of the airfoil where the low-pressure zone on the upper surface is located but away from the BLI engine, demonstrating the overall effect of the EDF on the entire low-pressure zone. Meanwhile, the second sample is closer to the BLI engine, studying the intake zone condition.

The result can be interpreted by investigating the separation results from VLM calculations of the MH-113 airfoil.

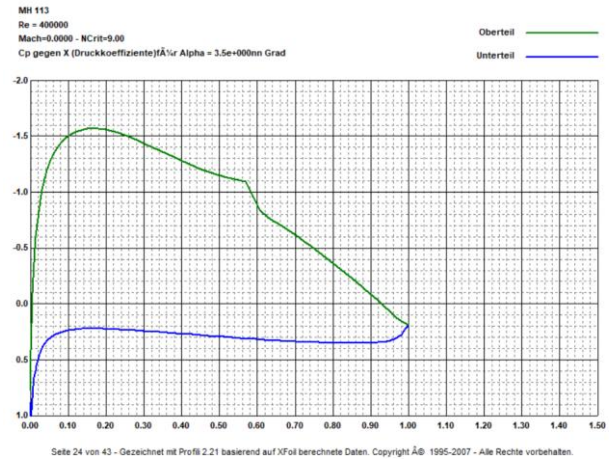

Figure 18. Pressure coefficients on MH-113.

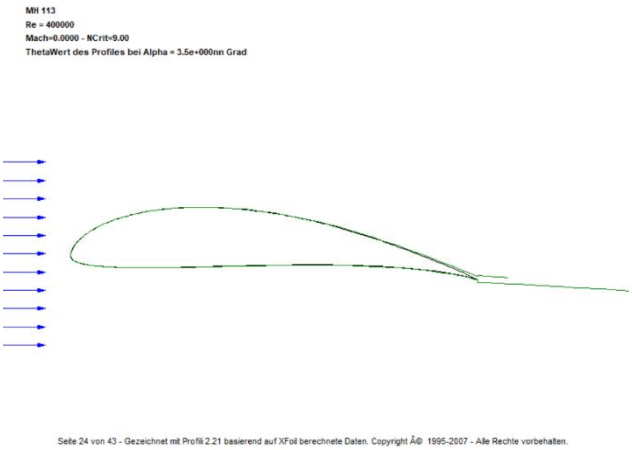

Figure 19. Pressure plot of MH-113 from Xfoil.

From the simulation, it can be indicated that the MH-113 generates lift from approximately 10% away from the trailing edge. Hence, installing the EDF too far in front will disrupt the original airflow. Meanwhile, as the EDF is oriented upwards, its negative pressure orientation can cause disruptions to the original flow field and even force separations while accelerating the flow, hence it can create contrary effects.

Meanwhile, after the critical *aoa* 3.5 degrees, the flow begins to separate from 10% before the trailing edge and even locations further towards the leading edge. Hence, placing the EDF too much backwards – negative 2.5% for example, will cause the EDF to ingest

already separated turbulent flow and will also hinder the boundary layer acceleration effect. The optimal solution lies between the two extreme cases.

The simulations yields the optimal value to be near the 5% position before the trailing edge. The estimated lift increase is 16.09% under cruising condition – a better improvement than the existing 10% [19].

D. Experiment Data

The wind visualization of a scenario is offered below along with simulation cut plot.

Figure 20. Wind Tunnel experiment with smoke visualization.

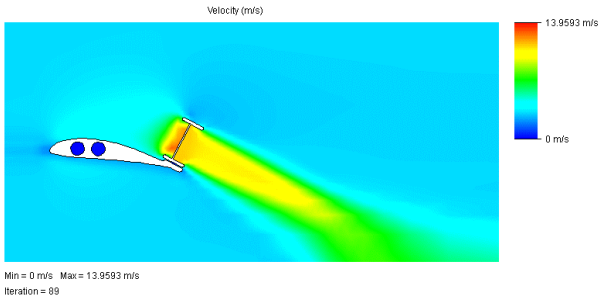

Figure 21. Compared simulation velocity cut plot.

The processed data and simulation data are demonstrated by the plot and table.

Table 2. Processed experimental data.

Exhaust (m/s)	P0	P1	P2	P3
0	3.051	4.305	3.709	2.671
5.7	3.041	4.456	4.771	5.694
11.1	3.038	4.783	6.081	7.449
13.8	3.061	4.876	6.769	10.81
16.6	2.985	4.962	7.452	14.26

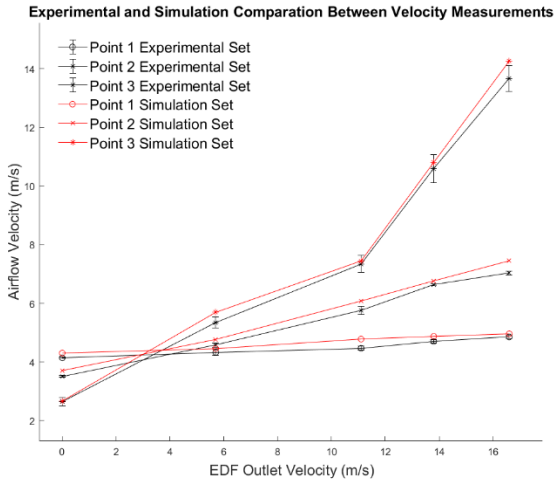

Figure 22. Plotted experimental data (black) and predicted data (red).

The simulation results show an average data variance of *2.4%* (maximal value 4.5%) and the simulation prediction varies with the experimental data by an average of *3.9%* (maximal value 7.0%).

The two sets of data indicate acceptable fitness and indicate the simulation results are valid as they fit with empirical values.

E. Environment Fitness Results

The friction force can be calculated by the kinetic friction formula given the coefficient [20]:

$$f = \mu_k \cdot N = 392.4N \cdot 0.2 = 78.48N$$

Considering the lift increase brought by the BLI engines, suppose that the aircraft takes off at 15% throttle during the taxi stage:

$$d_{taxi} = \frac{200}{165kg \cdot .15 - 37.1 \cdot .84 - 78.48} = 1.50m$$

The taxi distance fits STOL requirements while it can be further improved by using a larger current to take off if needed.

The researchers utilize a 120mm EDF with professional microphone to gain that the noise level at cruise rotation status is:

$$I_{unit} = 79 \pm 4\ dBA$$

The value is measured at 200mm away from the rotor. Hence the total noise created by the design is

$$I_0 = 79 + 10\log 16 = 91dBA$$

Assuming a cruise height of 80m (justified previously), and using the 6dB rule [16], the noise experienced by ground personnel as a result of the UAV is

$$I_g = I_o - 6 \cdot \log_2 \frac{h}{0.2m} = 39\text{dBA} < 50dBA$$

Hence, the operation of the UAV will not disturb people working below its path. According to the aforementioned 1:1.2 rule, it can be also inferred that the UAV will not bother residents living near the airfield.

F. *Cohort Results*

This section summarizes important results concerning the entire design as a whole.

Due to the utilization of the unique combination of tilted distributed BLI engines, this research reaches with several important improvements on important aerodynamic factors.

Table 3. Important cohort evaluations.

Factor	Improvement
Aerodynamic Efficiency	+16.09% (BLI)
Energy Efficiency	+9.40% (Ascending)
Propulsion Conservation	13.90% (Cruise)_
Ground Noise Level	~ 30dBA

Some important flight profile metrics of the UAV are given below.

Table 4. Important cohort flight metrics.

Factor	Number
Wingspan	4880mm
Endurance	1.55 hours @ 76kph
MTOW	40000g
Payload	16000g
Max Climb Rate	1:0.91
VC	20m/s

IV. Discussions

This section includes discussions on implications of results, possible errors and rooms for improvement, as well as a carbon emission mitigation case study.

A. *Implications of Results*

Aside from meeting design expectations specified in section I-D including flight profile, payload, and noise constraints, the innovative design features additional three main advantages:

- High aerodynamic performance. The UAV can operate a large attack and/or sideslip angles that other UAVs cannot, hence improving on its takeoff capability and maneuverability.
- High aerodynamic and energy efficiency, will conserve 13.90% of propulsion energy compared to conventional layouts. Meanwhile, its endurance and range are high, despite not being able to reach up to 200km. This makes the UAV a competitive solution for airspace transportation.
- Reliable and safe design. The UAV will be able to operate in cases of partial propulsion failure. There is abundant redundancy for propulsion units.

B. *Room for Improvement*

In terms of simulation and analytic works, although high precision has been achieved through a combination of CFD, empirical, and algebraic methods, some simulations are still made. For example, the simulated EDF units are simplified as velocity openings. Although it can reflect pressure conditions relatively well, it does not reflect trailing airflow realistically enough. Meanwhile, a full profile experiment is yet to be completed, which will be essential in the validation of the UAV's performance under more conditions.

In the experiment, despite rectification being done, the limited wind speed prevented the researchers from testing the wing under higher Reynold's numbers. Further experiments will be arranged in professional wind tunnels in university-ran institutions.

During the measurement, all measured values are smaller than the predicted ones. This can result from interference between the airflow measurement tool and the EDF - the tool will slightly disturb the airflow and slightly reduce the efficiency of the EDF, causing a lower measurement. This can be mitigated using other less intrusive instruments - such as pressure sensors.

Future research will focus on the full system development and control (without control surfaces) of the designed UAV to bring the solution to reality. Meanwhile, system engineering measures will be carried out to further enhance the range of the aircraft to be capable of covering all short-range branch line missions. Currently, scaled down models for test flights are under construction. While research improvements can and will be done, existing data has supported that the design is prospective and will prove successful regarding its scenario.

C. Case Study

Given data indicates that delivery points in urban communities typically receive 500 packages with an average weight of 2kg per day [21]. This requires 63 flights (with returns) per day to transport these cargos with the designed UAV. For distances between local delivery centers and community destinations, it typically takes the UAV roughly 1 hour 20 minutes to make a return trip. Given that Chinese delivery points typically work for 12 hours per day, at least five such UAVs will be allocated to transport the packages within the service time.

Suppose this transportation is made with conventional trucks, using the average emission data [22], each delivery point transportation will result in 20600g of carbon foot print per day. Even with electric cars, 15271g will be resulted. Using the UAV electric zero-emission solution, these carbon footprints will be eliminated.

Shanghai transported 3,741,379,000 packages per month according to data from past years [23]. Assuming 1000kg payloads for small trucks, these packages will result in approximately 1,946 tons of carbon footprint per month calculating with average data. Replacing the transportation of these packages with UAV formations, which are perfectly capable of satisfying the requirement within given time, will effectively reduce the carbon emission in the transportation industry.

V. Conclusion

With the initiative of reducing carbon emission in branch line express package transportation, this research focuses on the development of a new mid-sized STOL UAV based on tilted electric BLI engines using CFD and experiment affiliated with theoretical deductions in calculations, achieving an innovative zero-emission solution with a 16.09% increase in aerodynamic efficiency, 9.40% energy efficiency in ascension, 13.90% energy conservation during cruise, and up-to-standard noise level, capable of carrying 16kg of effective payload per flight with a maximum range of almost 120km.

The eventual results, both experimental and predicted, indicates that the newly proposed integration of the BLI technology will achieve a higher-level efficiency than existing BLI solutions. The system will also be able to effectively reduce carbon emissions in transportation and package delivery industries and can also be extended for applications in transportation in mountainous areas and more. The potential of this capable system is considerable in numerous industries, making transportation cleaner, faster, and more flexible.

VI. Acknowledgements

This research is completed by a team of two researchers. While H.S. is primarily in charge of completing designs, CFD simulations, and experiments, N.C. is responsible for data and analytics and partially for completing the report.

The research is carried out under the mentorship of Professor Daqing Huang and Professor Xingwei Kong.

While Prof. Huang has offered valuable guidance during experiments and analytical calculations as well as the writing process, Prof. Kong majorly discussed with the researchers the implementation and formation of the BLI design. Both mentors have provided this research with invaluable guidance.

REFERENCES

[1] *Express Industry Emissions*. https://www.greenpeace.org.cn/wp-content/uploads/2023/06/express-industry-emissions.pdf

[2] *CEICdata.com*. (2024, February 1). https://www.ceicdata.com.cn/zh-hans/china/transport-passenger-and-freight-average-distance

[3] Budziszewski, N. & Friedrichs, J. (2018). *Modelling of A Boundary Layer Ingesting Propulsor*. Institute of Jet Propulsion and Turbomachinery, TU Braunschweig, Hermann-Blenk-Straße 37, D-38108 Braunschweig, Germany.

[4] Zhang, X., Zhang, W., Li, W., Zhang, X., & Lei, T. (2022). *Experimental research on aero-propulsion coupling characteristics of a distributed electric propulsion aircraft*. Chinese Journal of Aeronautics.

[5] Kafantaris, K. (2023, September 8). *Boundary Layer Ingestion Propulsion*. Official: NASA. TBD.

[6] Celestina, M. L., & Long-Davis, M. J. (2019). *Large-Scale Boundary Layer Ingesting Propulsor Research*. NASA.

[7] Burton-Hughes, L. (2024, February 9). *Manual Handling Weight Limits: What are the Safe Lifting Guidelines and Techniques?* The Hub | High Speed Training.

[8] *DJI FlyCart 30 - Dynamic Aerial Delivery-DJI*. DJI. https://www.dji.com/cn/flycart-30

[9] *Soccer Court Standard Sizes and Facilitties Requirement*. https://www.dssysz.com/wenzhang/jishu/1694.html

[10] *Shanghai Buildings Height Layout*. Copyright © 2017 Sohu.com Inc. All Rights Reserved. https://www.sohu.com/a/143770307_119707

[11] *How to calculate Inter-Building distances in Shanghai?* https://zhishi.fang.com/xf/sh_301442.html

[12] *Plastic Track Standardized Sizes*. Copyright © 2017 Sohu.com Inc. All Rights Reserved. https://www.sohu.com/a/581090036_121289006

[13] *RSG White-Paper Drone-Noise Updated*. https://rsginc.com/wp-content/uploads/2021/12/RSG_White-Paper_Drone-Noise_Updated-12-2021.pdf

[14] *How loud are drones?* (Full drone noise breakdown). (2022, April 21). Dronesgator - Drone Review, Buyer Guides and Best Drones Lists. https://dronesgator.com/how-loud-are-drones/

[15] *SPREADING THE WORD: THE 6DB DECAY PER DOUBLE DISTANCE CHALLENGE*. - Yamaha - United States.

[16] *Free Shipping AEORC Patended Product Ducted Fan System EDF for Jet Plane* […]. (2021, January 11). DancingWingsHobby.

[17] *Turbines RC: EDF, RC models, airplanes, jets, RC parts and accessories for model aircrafts - TURBINES RC*.TURBINES RC. https://www.turbines-rc.com/

[18] *Tattu & Gens ace - RC Hobby FPV Heli UAV Lipo Battery.* https://www.genstattu.com/

[19] Szondy, D. (2017, November 9). *NASA harvests slow moving air to increase next-gen aircraft efficiency. New Atlas.* https://newatlas.com/nasa-starc-bli-engine/52112/

[20] Llc, E. E. *Coefficient of Friction Equation and Table chart.* https://www.engineersedge.com/coeffients_of_friction.htm

[21] *Logistics Q and A.* (2024, February 6). https://news.kdniao.com/logistics-qa/

[22] *China Ecology Net*. https://www.eco.gov.cn/news_info/64862.html

[23] *Shanghai Delivery Statics and Analysis*. https://zhuanlan.zhihu.com/p/527422904